

# Pareto Analysis of PI Tuning in Direct Digital Control of Multi-phase Drives<sup>\*</sup>

Manuel G. Satué<sup>\*</sup> J.D. Álvarez<sup>\*\*</sup> Manuel A. Perales<sup>\*\*\*</sup>

<sup>\*</sup> *Systems Engineering and Automation Department, University of Seville, 41092 Seville, Spain (e-mail: mgarrido16@us.es)*

<sup>\*\*</sup> *Department of Computer Engineering, Automation and Robotics, CIESOL—ceiA3, University of Almería, 04120 Almería, Spain (e-mail: jhervas@ual.es)*

<sup>\*\*\*</sup> *Electronic Engineering Department, University of Seville, 41092 Seville, Spain (e-mail: mperales@us.es)*

---

**Abstract:** PI tuning for variable-speed multi-phase drives is a complex task. In this paper, a Pareto analysis is introduced to reveal not previously reported links between figures of merit. The drive used for the study includes a 5-phase induction motor supplied by a voltage source inverter. A finite state predictive method is used for the inner loop (current control). The outer loop (speed control) is governed by a PI. The analysis is done experimentally thus including all sorts of non-idealities not appearing in commonly found models. The experimental results show how the pursuit for better performance is hindered by the existence of links between figures of merit. The importance of the result lies in showing that arbitrary performance enhancements are not possible in a general case.

*Keywords:* Application of power electronics, Digital implementation, Modeling and simulation of power systems, PI control, Tuning

---

## 1. INTRODUCTION

PI controllers are routinely used in variable speed drives for speed and/or current regulation. The speed control loop (outer loop) is used to maintain the mechanical speed close to its reference value. The current loop has a much faster time scale and is used to produce stator currents that, in turn, produce a torque that drives the speed. In the last years, there has been a trend in academia to replace PI loops with more sophisticated alternatives such as Model Predictive Control (MPC). This trend is a consequence of the relative success attained by MPC in other realms (Berenguel et al., 1998; Ramírez-Arias et al., 2005). The case of predictive control of drives is exemplified by the so called Finite State Model Predictive Control (FSMPC), where direct digital control of the Voltage Source Inverter (VSI) is attained. In FSMPC the Pulse Width Modulation (PWM) stage is no longer necessary, thus improving the performance of the system as reported by Lim et al. (2013); Bermúdez et al. (2020).

Going back to the speed control loop, the influential works related to PI tuning for Indirect Field Oriented Control (IFOC) date from the 1990s and 2000s (De Wit et al., 1996; Espinosa-Perez and Ortega, 1997; Espinosa-Perez et al., 1998; Bazanella and Reginatto, 2001). These works pro-

vide methods which utilize some, not very strict, requirements on the knowledge of the time constant of the rotor of the IM to guarantee the global stability. A dynamic model of the current fed IM is used at the basis of these methods. Some variations have been reported making use of harmonic injection (Arahal and Duran, 2009), but, in most cases, the models do not consider practicalities like nonlinearities in the IM dynamics, VSI+modulation behavior and aspects derived from the use of a Digital Signal Processor (DSP) for the PI + IFOC algorithms.

In the 20 years that followed, the state of the art has been enriched by some papers expanding the previous works in a variety of ways. Most of the efforts have focused on: sensorless operation, estimation of the rotor time constant, extension of the PI with operating-point based scheduling and/or adaptivity, fault-tolerant capabilities, and tuning methods based on extensive simulation/experimentation. Other technologies have even been proposed to replace the speed PI but, despite all of this, conventional PI control is still reported as competitive due to its simple implementation compared with nonlinear control (Ortega et al., 1993), adaptive control (Marino et al., 1993), robust control (Ding et al., 2000; Alamo et al., 2006) and some fuzzy and/or neural approaches (Masiala et al., 2008; Pham and Le, 2020). The lack of theoretical models to analyze the above cited practical aspects and their influence on complex figures of merit such as the Integral Time-multiplied Absolute Error (ITAE) has led to the use of an experimental approach for the PI tuning. For example, in Shaija and Daniel (2023) metaheuristic optimisation algorithms are used for the optimal PI tuning. Again, MPC

---

<sup>\*</sup> This work is part of the Grant TED2021-129558B-C22 funded by MCIN/AEI/10.13039/501100011033 and by the “European Union NextGenerationEU/PRTR”. Also, the authors want to thank the support provided by project I+D+i/PID2021-125189OB-I00, funded by MCIN/AEI/10.13039/501100011033/ by “ERDF A way of making Europe”.

schemes are able to consider more complex models, being this another reason for its proposal (Arahall et al., 2008).

Moreover, in recent years, there has been a technological advance in the drives themselves. The motors have moved from 3-phase IMs to multi-phase machines and from two-level to multi-level VSIs (Rodríguez et al., 2023). The multi-phase case is specially interesting for this study as the overall structure of the controller is IFOC-like. The interaction among phases makes the tuning of the inner loop PIs more complex. Multi-phase drives requires at least 4 PI controllers for the PWM method and just one predictive controller for FSMPC. In particular, the existence (in stator currents of multi-phase IM) of a torque producing plane ( $\alpha-\beta$ ) and various harmonic planes ( $x_j-y_j$  with  $j \geq 1$ ) makes the control design more challenging. For instance, modulation schemes for 6 and 5-phase drives have little to do with each other, yet predictive controllers have the same structure for both. So, FSMPC has rendered the problem more tractable but at the cost of higher computational needs (Gonçalves et al., 2019; Martín et al., 2016). Also, the FSMPC method is becoming popular for its flexibility. For instance, modulation variants that are impossible with PWM can be used with FSMPC (Satué et al., 2023; Zhang et al., 2023), the mechanical load characteristics can be considered with ease, and fault-tolerance capabilities are better utilized (Yepes et al., 2022). State estimation methods such as Kalman filtering and observers can also be incorporated with ease in MPC approaches (Bermudez et al., 2020; Cecilia and Costa-Castelló, 2020), expanding its potential with respect to the PI case.

Speed PI tuning can, in theory, make use of an accurate model of the IM. However, some aspects have been resistant to modelling. This is the case of the delay introduced by the modulation technique used (PWM or its variants or even FSMPC). Saturation in some variables (currents, fluxes, etc.) have also not been considered in many cases (Toral et al., 2010). Finally, some figures of merit such as torque ripple are typically not considered in the automatic control community, yet they play a crucial role in applications. In this context there is not a set of equations (or other convenient procedure) to link figures of merit with controller parameters. The proposal of this paper consider a reduced set of indices to assess controllers for the inner loop of drives. These indices summarize the system's behavior as other indices are related to the set. Then, all possible controller tunings are considered. The Pareto-optimal solutions are then show to pertain to a surface of lower dimension. As a result, any PI tuning must either be dominated (not Pareto-optimal) or lie in the surface.

## 2. IFOC STRUCTURE USED IN THE EXPERIMENTS

In the indirect field-oriented control scheme flux and torque are independently regulated. The flux current set point  $i_d^*$  is set to magnetize the motor whereas quadrature current  $i_q^*$  is used to manipulate the produced torque. The PI in the velocity feedback loop is responsible for generating  $i_q^*$  to drive the mechanical speed control error to zero.

$$i_q^*(t) = k_p \cdot e(t) + k_i \int_0^t e(\tau) d\tau \quad (1)$$

where  $e = \omega^* - \omega^e$  is the velocity error or difference between the speed set point ( $\omega^*$ ) and the speed measurement ( $\omega^e$ ).

Once the set-points in  $d-q$  coordinates are known, they are projected to the  $\alpha-\beta$  space using the Park transformation, obtaining a reference for stator current in  $\alpha-\beta$  plane as  $I_{\alpha-\beta}^* = D (i_d^*, i_q^*)^\top$ , where matrix  $D$  is given by

$$D = \begin{pmatrix} \cos(\theta_a) & \sin(\theta_a) \\ -\sin(\theta_a) & \cos(\theta_a) \end{pmatrix} \quad (2)$$

The flux position  $\theta_a$  is estimated as  $\theta_a = \int \omega_e dt$  where  $\omega_e = \omega_{sl} + P\omega$ , being  $P$  is the number of pairs of poles of the induction machine,  $\omega$  the mechanical speed and

$$\omega_{sl} = \frac{i_q^*}{i_d^*} \frac{1}{\hat{\tau}_r} \quad (3)$$

where  $\hat{\tau}_r$  is an estimation of the rotor time constant  $\tau_r = L_r/R_r$ . As a result, the set point for stator current tracking  $i^*(k)$  has an amplitude  $I^* = \sqrt{i_d^{*2} + i_q^{*2}}$ . Finally, the  $\alpha-\beta$  references can be expressed as  $i_\alpha^*(t) = I^* \sin \omega_e t$ ,  $i_\beta^*(t) = I^* \cos \omega_e t$ ,  $i_x^*(t) = 0$ ,  $i_y^*(t) = 0$ , where  $i_x^*$  and  $i_y^*$  are currents related to losses in the harmonic plane  $x-y$ .

### 2.1 FSMPC Control of a 5-phase IM

The inner loop of an IFOC scheme is responsible for producing stator currents in  $\alpha-\beta$  that follows their references and, at the same time, maintaining  $x-y$  currents close to zero as they do not produce torque but contribute to losses. This task can be accomplished using the FSMPC strategy. A model of the IM is needed to predict the IM behavior for each possible VSI configuration. Using the vector space decomposition, the 5-phase stator currents are projected to the energy conversion ( $\alpha-\beta$ ) plane and harmonic ( $x-y$ ) plane, resulting in equations relating stator voltages  $v_s(t)$ , stator and rotor currents  $i_s(t)$ ,  $i_r(t)$ , fluxes  $\Psi_s(t)$ ,  $\Psi_r(t)$  and rotor electrical angular speed  $\omega_r(t)$  as follows.

$$\begin{aligned} v_{\alpha\beta s}(t) &= R_s i_{\alpha\beta s}(t) + p\Psi_{\alpha\beta s}(t) \\ 0 &= R_r i_{\alpha\beta r}(t) + p\Psi_{\alpha\beta r}(t) - j\omega_r(t)\Psi_{\alpha\beta r}(t) \\ \Psi_{\alpha\beta s}(t) &= L_s i_{\alpha\beta s}(t) + L_m i_{\alpha\beta r}(t) = L_s i_{\alpha\beta s}(t) + L_m i_{\alpha\beta r}(t) \\ \Psi_{\alpha\beta r}(t) &= L_m i_{\alpha\beta s}(t) + L_r i_{\alpha\beta r}(t) = L_m i_{\alpha\beta s}(t) + L_r i_{\alpha\beta r}(t) \\ v_{xy s}(t) &= R_s i_{xy s}(t) + p\Psi_{xy s}(t) \\ \Psi_{xy s}(t) &= L_{ls} i_{xy s}(t) \end{aligned} \quad (4)$$

where  $p$  is the derivative operator, and the following machine parameters are used: resistances  $R_s$ ,  $R_r$ , inductances  $L_s$ ,  $L_r$ , leakage inductance  $L_{ls}$  and mutual inductance  $L_m$ . Sub-index  $s$  stands for stator and  $r$  for rotor. The stator voltages are produced by the VSI according to the gating signals  $K_j$  for VSI legs  $j = 1, \dots, 5$  accommodated in  $\mathbf{u} = (K_1, \dots, K_5) \in \mathbb{B}^5$  with  $\mathbb{B} = \{0, 1\}$ . The resulting voltages  $\mathbf{v}_{\alpha\beta xy s}$  are

$$\mathbf{v}_{\alpha\beta xy s} = (v_{\alpha s}, v_{\beta s}, v_{x s}, v_{y s}) = V_{DC} \mathbf{u} \mathbf{T} \mathbf{M} \quad (5)$$

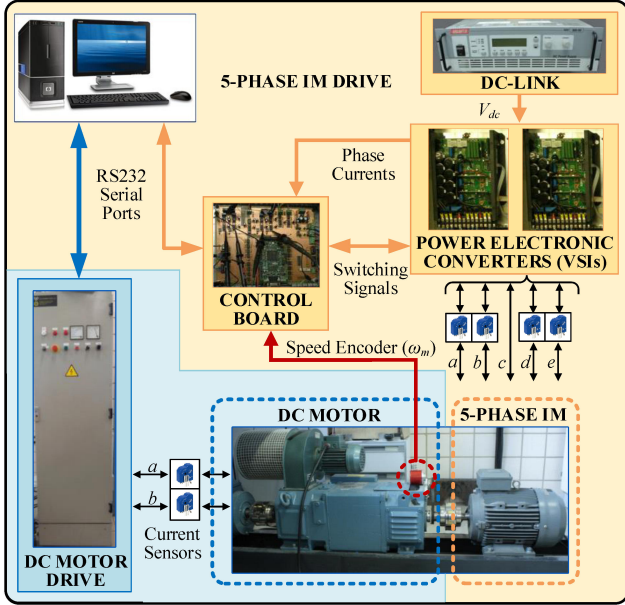


Fig. 1. Diagram and photographs of the laboratory setup used in the experiments.

where  $V_{DC}$  is the DC link voltage,  $\mathbf{T}$  a connectivity matrix and  $\mathbf{M}$  a coordinate transformation matrix accounting for the spatial distribution of machine windings.

$$TM = \begin{pmatrix} a & b & b & b & b \\ b & a & b & b & b \\ b & b & a & b & b \\ b & b & b & a & b \\ b & b & b & b & a \end{pmatrix} \cdot \begin{pmatrix} d & \gamma_1^c & \gamma_2^c & \gamma_3^c & \gamma_4^c \\ 0 & \gamma_1^s & \gamma_2^s & \gamma_3^s & \gamma_4^s \\ d & \gamma_2^c & \gamma_4^c & c_\vartheta & \gamma_3^c \\ 0 & \gamma_2^s & \gamma_4^s & \gamma_1^s & \gamma_3^s \\ c & c & c & c & c \end{pmatrix} \quad (6)$$

The coefficients used are:  $a = 4/5$ ,  $b = -1/5$ ,  $c = -b$ ,  $d = 2/5$ ,  $\gamma_h^c = \cos h\vartheta$ ,  $\gamma_h^s = \sin h\vartheta$  and  $\vartheta = 2\pi/5$  for the five-phase IM. The actual values of the electrical parameters corresponding to the machine used in the experiments are given in Table 1.

At discrete-time  $k$ , the control action  $\mathbf{u}(k+1)$  is computed minimizing a cost function  $J$ . The cost function penalizes stator currents tracking error as  $J = \|\hat{i}^*(k+2) - \hat{i}(k+2)\|^2$ , where  $\hat{i}(k+2)$  are the predicted currents. Note the one sampling period delay due to computations.

The developed mechanical torque is derived from the actual values of the direct and quadrature stator currents as

$$T = P \frac{L_m^2}{L_{lr} + L_m} i_d \cdot i_q. \quad (7)$$

### 3. EXPERIMENTS

The PI tuning is assessed in this section by means of tests in the experimental setup described below.

#### 3.1 Laboratory Setup

The laboratory arrangement depicted in Fig. 1) is used. A five-phase motor with parameters shown in table 1 is

Table 1. Parameters of the five-phase IM

Parameter	Value	Unit
Stator resistance, $R_s$	12.85	$\Omega$
Rotor resistance, $R_r$	4.80	$\Omega$
Stator leakage inductance, $L_{ls}$	79.93	mH
Rotor leakage inductance, $L_{lr}$	79.93	mH
Mutual inductance, $L_M$	681.7	mH
Rotational inertia, $J_m$	0.02	kg m <sup>2</sup>
Number of pairs of poles, $P$	3	-

powered by a five-phase VSI constructed from two three-phase SEMIKRON SKS 22F modules. A 300V DC power supply is used in the DC-link. The control programs run on a MSK28335 board housing a TMS320F28335 DSP. Hall effect sensors (LH25-NP) are used to measure the stator phase currents. Last, a DC motor sharing the same axis as the IM is used to provide an opposing torque load ( $T_L$ ) for the tests.

#### 3.2 Performance indices

The assessment of variable speed drives can be based on a variety of quantitative criteria. Different applications might put more emphasis on some indices over others. In this paper three indices are selected. The proposed indices can be obtained experimentally from a step test. The first one is the percentage overshoot  $PO$ , defined for an underdamped system as

$$PO = 100 \cdot \frac{\max \omega - \omega^*}{\omega^*} \quad (8)$$

The second index is the rise time (from 0% to 100%) defined as the time needed to cross the  $\omega^*$  value for the first time.

$$RT = \operatorname{argmin}_{t \geq 0} \omega^*(t) - \omega(t) \quad (9)$$

The final index is the torque ripple, that is defined as

$$QR = \sqrt{\frac{1}{N} \sum_{k=1}^N (T^*(k) - T(k))^2} \quad (10)$$

The set of all three indices will be represented as vector

$$\Gamma = (PO, RT, QR) = (\gamma_1, \gamma_2, \gamma_3) \quad (11)$$

The units of  $\gamma_1$ ,  $\gamma_2$  and  $\gamma_3$  are %, s and N · m respectively.

#### 3.3 Pareto Surface

A set of step tests are performed on the 5-phase IM to obtain the figures of merit for various combinations of the PI parameters ( $k_p$ ,  $k_i$ ). The obtained triples  $\Gamma$  for each PI tuning are recorded. Then, a process of elimination is used to exclude the triples that are not Pareto-optimal. The surviving ones are presented in Fig. 2 where a 3D plot (upper right corner) shows the  $\Gamma$  values and three 2D projections show:  $\gamma_2$  vs.  $\gamma_1$  (upper left),  $\gamma_3$  vs.  $\gamma_1$  (lower left) and  $\gamma_3$  vs.  $\gamma_2$  (lower right). The points are presented with color for better visualization. The color has been

Table 2. Optimal tunings for different operating points

$\omega^*$	$k_p^0 \cdot 10^3$	$k_i^0 \cdot 10^5$	$\gamma_1^0$	$\gamma_2^0$	$\gamma_3^0$	$\bar{\Pi}$
500	65	100	3.3	0.17	0.0120	0.0148
375	42	107	5.3	0.17	0.0103	0.0114
250	120	80	7.1	0.11	0.0123	0.0123
125	130	60	12.9	0.09	0.0101	0.0224

linked to  $\gamma_3$  to provide a sense of elevation. A red color indicates a high value of  $\gamma_3$  and blue color indicate low value of  $\gamma_3$ .

It is interesting to see that the  $\Gamma$  triples are situated approximately on a cubic Titeica surface (Tzitzéica, 1908). The surface is determined mathematically by

$$\gamma_1 \cdot \gamma_2 \cdot \gamma_3 = \bar{\Pi} \quad (12)$$

where  $\bar{\Pi} = 0.0148$  for this case. The repercussions of this findings are deep: by PI tuning alone it is impossible to enhance all figures of merit simultaneously past the Pareto front. Since  $\gamma_1 \cdot \gamma_2 \cdot \gamma_3$  is (approximately) a constant, reducing  $\gamma_1$  will result in an increase in  $\gamma_2 \cdot \gamma_3$ . The same argument holds for a reduction in either  $\gamma_2$  or  $\gamma_3$ .

Going back to the tuning problem, it is interesting to notice that a particular point in the Pareto front minimizes the distance to the origin. This particular solution ( $\Gamma^0$ ) achieves

$$\|\Gamma^0\|^2 = \min(\gamma_1^2 + \gamma_2^2 + \gamma_3^2) \quad (13)$$

This solution is optimal if the control objectives (figures of merit) are equally important. This might not be the case in a practical application. A weighted metric should be used instead. This is easily achieved by applying scale factors to each figure of merit. For the sake of clarity the distance of equation (13) will be used. In this case the solution closest to the origin (denoted as  $\Gamma^0$ ) is found to be  $\Gamma^0 = (3.3, 0.17, 0.0120)$ . If one chooses to tune the PI to achieve  $\Gamma^0$ , the tuning problem has a definite answer. This is a step forward from various previous works where the existence of limits for tuning is not realized.

### 3.4 Influence of the operating regime

So far, just an operating point has been analyzed. The method is now extended to other values of  $\omega^*$  to check to what extent the Pareto surface and optimal tuning are affected.

Fig. 3 presents the Pareto front and its projections for  $\omega^* = 250$  (rpm). It can be seen that the Pareto-optimal solutions still lie (approximately) in a Titeica surface. However, for this operating point, the figures of merit have different values. This can be seen comparing Fig. 2 with Fig. 3 and also in table 2. In said table, various speed references are considered. For each one the PI tuning that yields  $\Gamma^0$  is provided along the actual values of  $\gamma_i^0$  and the  $\bar{\Pi}$  parameter. It can be seen that the optimal tuning is different for each operating point. This support the adoption of scheduling solutions such as in Arahall et al. (2019).

In most cases, however, a single PI tuning is uses. The particular tuning can be found by trial and error aiming at

Table 3. Comparison of results in different operating points

$\omega^*$	Tuning	$\gamma_1^0$	$\gamma_2^0$	$\gamma_3^0$
500	T1	3.92	0.177	0.0281
500	T2	3.98	0.168	0.0283
375	T1	5.25	0.152	0.0290
375	T2	5.34	0.141	0.0295
250	T1	7.37	0.131	0.0289
250	T2	7.34	0.119	0.0293
125	T1	13.77	0.128	0.0277
125	T2	13.83	0.109	0.0284

improving performance near the nominal operating point. This of course has the effect of diminished performance far from said nominal point. This is illustrated by table 3 where two PI tunings are compared in terms of the figures of merit for each speed regime. Tuning T1 corresponds to the optimal tuning for 500 rpm ( $k_p = 65 \cdot 10^3$ ,  $k_i = 100 \cdot 10^5$ ), whereas T2 uses as PI parameters the mean value over the various speed regimes, producing ( $k_p = 89 \cdot 10^3$ ,  $k_i = 86 \cdot 10^5$ ). It can be seen that the results are not so different and the degradation with respect to the optimal case might be acceptable in many applications. This provides support for the usual engineering practice used for tuning. However, for high end applications, the results of this paper show that PI tuning has limits and that something else is needed to provide high performance in all operating points. This is a powerful result that can not be arrived at without the Pareto analysis.

## 4. CONCLUSION

Assessment of controllers is presented in many works by means of a few cases. The results of this paper show that such procedure is insufficient because two important issues are kept in the dark. First, the trade-offs between figures of merit, and second the relationship between optimal tuning and operating regimes. Without a complete Pareto analysis covering all operating regimes the conclusions are necessarily baseless.

## ACKNOWLEDGEMENTS

This work is part of the Grant TED2021-129558B-C22 funded by MCIN/AEI/10.13039/501100011033 and by the “European Union NextGenerationEU/PRTR”. Also, the authors want to thank the support provided by project I+D+i/PID2021-125189OB-I00, funded by MCIN/AEI/10.13039/501100011033/ by “ERDF A way of making Europe”.

## REFERENCES

- Alamo, T., Normey-Rico, J.E., Arahall, M.R., Limon, D., and Camacho, E.F. (2006). Introducing linear matrix inequalities in a control course. *IFAC Proceedings Volumes*, 39(6), 205–210.
- Arahall, M.R., Cirre, C.M., and Berenguel, M. (2008). Serial grey-box model of a stratified thermal tank for hierarchical control of a solar plant. *Solar Energy*, 82(5), 441–451.
- Arahall, M.R., Kowal, G., Barrero, F., and del Mar Castilla, M. (2019). Cost function optimization for multi-phase induction machines predictive control.

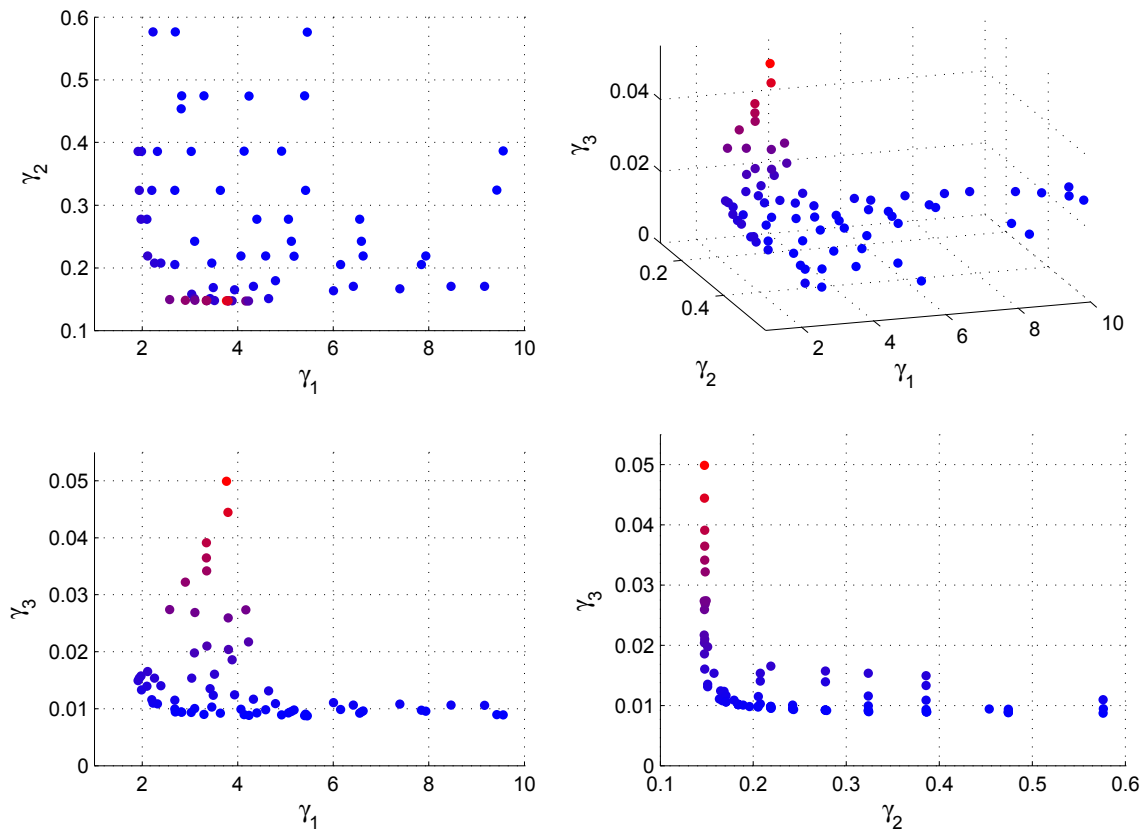


Fig. 2. Pareto front (upper right corner) and 2D projections for  $\omega^* = 500$  (rpm). Color is used to indicate  $\gamma_3$  values for better visualization.

*Revista Iberoamericana de Automática e Informática Industrial*, 16(1), 48–55.

- Arahal, M. and Duran, M. (2009). PI tuning of five-phase drives with third harmonic injection. *Control Engineering Practice*, 17(7), 787–797.
- Bazanella, A.S. and Reginatto, R. (2001). Robust tuning of the speed loop in indirect field oriented control of induction motors. *Automatica*, 37(11), 1811–1818.
- Berenguel, M., Arahal, M., and Camacho, E. (1998). Modelling the free response of a solar plant for predictive control. *Control Engineering Practice*, 6(10), 1257–1266.
- Bermudez, M., Arahal, M.R., Duran, M.J., and Gonzalez-Prieto, I. (2020). Model predictive control of six-phase electric drives including arx disturbance estimator. *IEEE Transactions on Industrial Electronics*, 68(1), 81–91.
- Bermúdez, M., Martín, C., González-Prieto, I., Durán, M.J., Arahal, M.R., and Barrero, F. (2020). Predictive current control in electrical drives: an illustrated review with case examples using a five-phase induction motor drive with distributed windings. *IET Electric Power Applications*, 14(8), 1291–1310.
- Cecilia, A. and Costa-Castelló, R. (2020). High gain observer with dynamic deadzone to estimate liquid water saturation in PEM fuel cells. *Revista Iberoamericana de Automática e Informática industrial*, 17(2), 169–180.
- De Wit, P.A., Ortega, R., and Mareels, I. (1996). Indirect field-oriented control of induction motors is robustly

globally stable. *Automatica*, 32(10), 1393–1402.

- Ding, G., Wang, X., and Han, Z. (2000).  $H_\infty$  disturbance attenuation control of induction motor. *International Journal of Adaptive Control and Signal Processing*, 14(2-3), 223–244.
- Espinosa-Perez, G., Chang, G., Ortega, R., and Mendes, E. (1998). On field-oriented control of induction motors: Tuning of the PI gains for performance enhancement. In *Proceedings of the 37th IEEE Conference on Decision and Control (Cat. No. 98CH36171)*, volume 1, 971–976. IEEE.
- Espinosa-Perez, G. and Ortega, R. (1997). Tuning of PI gains for FOC of induction motors with guaranteed stability. In *Proceedings of the IECON'97 23rd International Conference on Industrial Electronics, Control, and Instrumentation (Cat. No. 97CH36066)*, volume 2, 569–574. IEEE.
- Gonçalves, P., Cruz, S., and Mendes, A. (2019). Finite control set model predictive control of six-phase asymmetrical machines—an overview. *Energies*, 12(24), 4693.
- Lim, C.S., Levi, E., Jones, M., Rahim, N.A., and Hew, W.P. (2013). FCS-MPC-based current control of a five-phase induction motor and its comparison with PI-PWM control. *IEEE Transactions on Industrial Electronics*, 61(1), 149–163.
- Marino, R., Peresada, S., and Valigi, P. (1993). Adaptive input-output linearizing control of induction motors. *IEEE Transactions on Automatic control*, 38(2), 208–

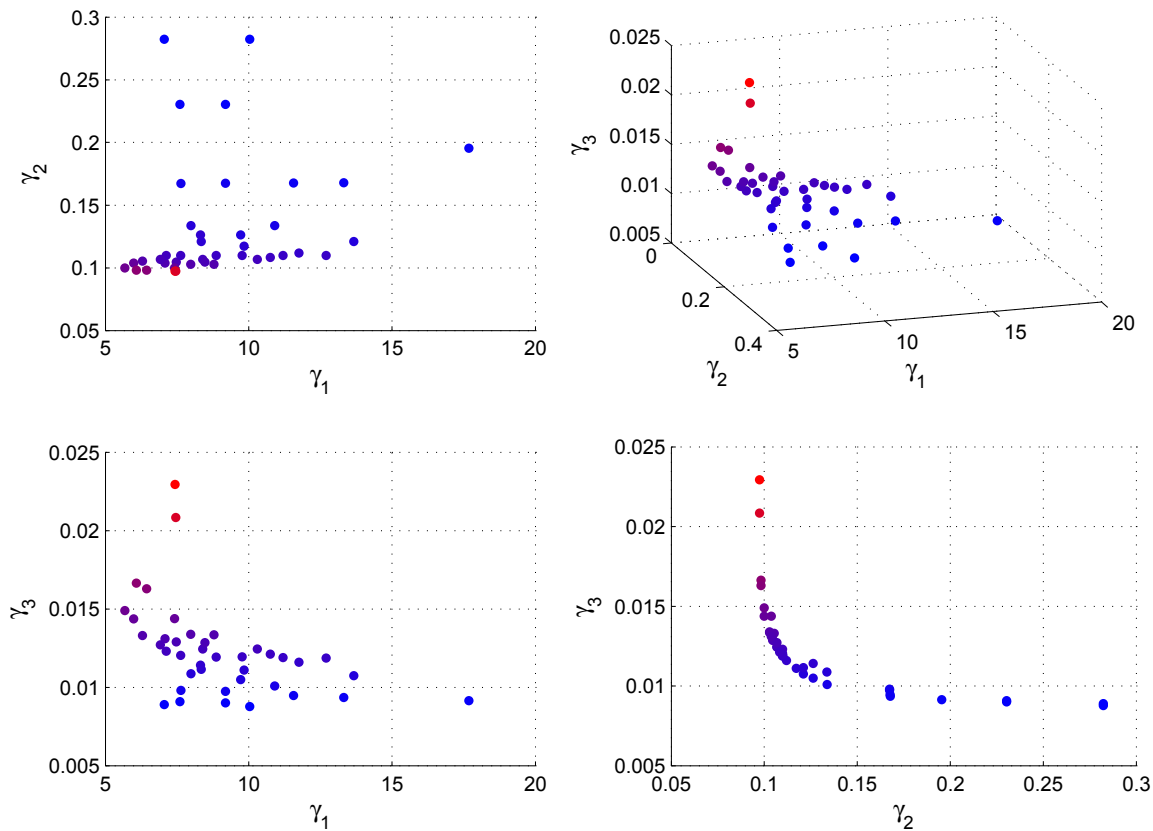


Fig. 3. Pareto front (upper right corner) and 2D projections for  $\omega^* = 250$  (rpm). Color is used to indicate  $\gamma_3$  values for better visualization.

- 221.
- Martín, C., Arahal, M.R., Barrero, F., and Durán, M.J. (2016). Multiphase rotor current observers for current predictive control: A five-phase case study. *Control Engineering Practice*, 49, 101–111.
- Masiala, M., Vafakhah, B., Salmon, J., and Knight, A.M. (2008). Fuzzy self-tuning speed control of an indirect field-oriented control induction motor drive. *IEEE Transactions on Industry Applications*, 44(6), 1732–1740.
- Ortega, R., Canudas, C., and Seleme, S.I. (1993). Nonlinear control of induction motors: Torque tracking with unknown load disturbance. *IEEE Transactions on Automatic Control*, 38(11), 1675–1680.
- Pham, N.T. and Le, T.D. (2020). Novel FOC vector control structure using RBF tuning PI and SM for SPIM drives. *International Journal of Intelligent Engineering & Systems*, 13(5).
- Ramírez-Arias, A., Rodríguez, F., Guzmán, J.L., Arahal, M.R., Berenguel, M., and López, J.C. (2005). Improving efficiency of greenhouse heating systems using model predictive control. *IFAC Proceedings Volumes*, 38(1), 40–45.
- Rodríguez, F., Garrido, D., Núñez, R., Oggier, G.G., and García, G. (2023). Feedback linearization control of a dual active bridge converter feeding a constant power load. *Revista Iberoamericana de Automática e Informática industrial*, 237–246.
- Satué, M.G., Arahal, M.R., Ramírez, D.R., and Barrero, F. (2023). Multi-phase predictive control using two virtual-voltage-vector constellations. *Revista Iberoamericana de Automática e Informática industrial*, 01–05.
- Shaija, P. and Daniel, A.E. (2023). Optimal tuning of PI controllers for IM drive using GWO and TLBO algorithms. In *2023 Fifth International Conference on Electrical, Computer and Communication Technologies (ICECCT)*, 01–09. IEEE.
- Toral, S.L., Torres, M.M., Barrero, F., and Arahal, M.R. (2010). Current paradigms in intelligent transportation systems. *IET Intelligent Transport Systems*, 4(3), 201–211.
- Tzitzéica, M.G. (1908). Sur une nouvelle classe de surfaces. *Rendiconti del Circolo Matematico di Palermo (1884-1940)*, 25(1), 180–187.
- Yepes, A.G., Lopez, O., Gonzalez-Prieto, I., Duran, M.J., and Doval-Gandoy, J. (2022). A comprehensive survey on fault tolerance in multiphase AC drives, part 1: General overview considering multiple fault types. *Machines*, 10(3), 208.
- Zhang, H., Zhang, Y., Zhu, Y., and Wang, X. (2023). Robust deadbeat predictive current control of induction motor drives with improved steady state performance. *IET Power Electronics*.